

## Young Stellar Clusters in the Outer Galaxy

Zhibo Jiang, Min Fang, and Ji Yang

*Purple Mountain Observatory, Chinese Academy of Sciences, Nanjing 210008, China*

zbjiang@pmo.ac.cn, mfang@pmo.ac.cn, jiyang@pmo.ac.cn

### ABSTRACT

We have carried out a near-infrared broad band survey toward the regions that are associated with high velocity carbon monoxide molecular gas. These regions are located outside the solar circle. Of the 76 regions observed, 45 show congregations of young stellar objects. The color images composed of JHKs band images the cluster regions are presented. The clusters studied here display a variety of morphologies and near-infrared colors. Some properties, such as the memberships, stellar surface densities, the Ks magnitudes of the brightest stars are derived and presented. The photometric data suggest that about one-half of the regions may contain massive stars. We have also derived some statistical properties of the region. The Ks-band luminosity function composed of a subset of the presented clusters is quite similar to that of typical young stellar clusters, suggesting the initial mass function are of the similar form, though the clusters are distributed in a wide range in the Galaxy. Further analysis suggests that the mass of the most massive star in a cluster is related more to the numbers of the members and the radii than to the surface densities of the cluster.

*Subject headings:* infrared: stars—stars: formation—stars: pre-main sequence—surveys

## 1. Introduction

Most stars are believed to be born in congregations and die solitarily. That means that most stars spend their early lives in clusters, referred to as Young Stellar Clusters (YSCs) or embedded clusters. While the formation and early evolution of isolated low-mass stars has been well studied, how stars are formed and spend their early lives in cluster environments is still less clear. Moreover, massive stars, whose formation process is still under dispute, are all associated with clusters. Though massive stars contribute a small fraction of total mass (Salpeter 1955; Scalo 1998), they emit a vast majority of lights in the universe, thus have more profound effects on the evolution of the universe than low-mass stars. Therefore, studying how clusters are formed and evolve will provide very important information of the evolution of our Galaxy as well as of the universe.

With the advent of large format infrared detectors in late 1980's, enormous progress has been made on the study of YSCs. To date, several hundreds of YSCs have been detected and cataloged (Bica, Dutra, & Barbuy 2003; Lada & Lada 2003; Porras et al. 2003). Tens of these clusters have been intensively studied by means of NIR imaging and spectroscopy (e.g., Greene & Meyer 1995; Lada & Lada 1995; Hillenbrand 1997). These studies have enabled us to understand the typical properties of YSCs. However, though a large number of YSCs have been discovered and studied, the studies are far from being complete. Assuming a star forming rate of  $2\text{--}3 M_{\odot} \text{ yr}^{-1}$  in the Galaxy (Lada 1999), and an average mass of  $500 M_{\odot}$  for YSCs (Lada & Lada 2003), we can estimate that  $\sim 4 \times 10^4$  YSCs with less than 10 Myr age in the Galaxy. That is to say, only a small part of the YSCs in the Galaxy have been discovered. This hampers us from knowing some of the statistical properties of YSCs. It is therefore very important to expand our samples in order to understand the formation and evolution of stellar clusters.

A pioneer work of searching for YSCs had been done by Hodapp (1994), who carried

out a  $K'$ -band survey towards molecular outflow regions (Fukui 1989) and found a significant number of YSCs. Inspired by the success of that work, we started a NIR survey towards outflow candidate regions. In a previous survey of CO(J=1,0) molecular line, these regions show high velocity wings (Yang et al. 2002). Probably they are in an active phase of star formation. About one-third of the outflow candidate regions have been observed in the near infrared. We detected over forty infrared stellar clusters or small groups. This paper presents the preliminary results of the survey.

## 2. Observation and Data Reduction

The observations were carried out in the winters of 1999–2002, which are 1999 November, 2000 November, 2001 December and 2002 January, respectively. However, only observations in January 2002 yields most of the data. We used OASIS mounted on the OAO 1.88m telescope(Okumura et al. 2000) to carry out the observation. Typical weather of observing nights were not so good. Sometimes the weather condition changed quickly, resulting in a relatively large photometric errors. We estimate photometric errors for some regions could be as large as 0.5 mag. Generally we took exposures in JHKs-bands for each region, but for some regions there are no H-band data. For each region, typically five dithered frames have been taken with exposure time of J $\sim$ 30 s, H $\sim$ 10-20 s and Ks $\sim$ 10 s for each frame, based on the weather condition and sky background level. The total exposure times are usually J $\sim$ 150 s, H $\sim$ 90 s and Ks $\sim$ 50 s, making  $10\sigma$  limiting magnitudes of J $\sim$ 17.5,H $\sim$ 16.8 and Ks $\sim$ 16.0.

All data were reduced in IRAF packages in a usual manner. The images were dark-subtracted, flat-fielded. Then each image was subtracted by the sky image constructed by median combination of dithered frames. Then the dithered frames of each region were aligned and combined to make an image with higher s/n ratio.

The photometry has been done by tasks in the DAOPHOT package. The routine work is similar as described in Jiang et al. (2002) and will not be stated redundantly here. The typical aperture radius used in the photometry is  $2.9''$  (3 pixels). The fluxes are calibrated by standard NIR sources listed in Hunt et al. (1998), which were selected close to the target regions and observed after every three or four target observations. The images of the standards were reduced nearly in the same way as those of the targets, but not aligned and combined. The fluxes of the standards were calculated for each image and averaged to obtain the final magnitude correction. The instrumental correction was estimated by comparing the aperture photometric results between using an aperture of 3 pixels and of 15 pixels. We found that in most regions 3-pixel aperture can cover 90% of the total flux and corrected all the photometric result accordingly. The astrometry of the point sources were calibrated by the 2MASS and UNNO database. To make statistical sense, the completeness limiting magnitude is essential. We estimated the completeness limiting magnitude by adding and searching artificial stars to some images. The typical value is about 15.5 in the Ks-band.

### 3. Results

Totally we have observed 76 regions which showed high velocity CO molecular line emission. Of the 76 regions, 45 ( $\sim 60\%$ ) regions are associated with stellar groups or clusters. Two regions, i.e. AFGL 5157 and AFGL 5142, which were observed previously (Chen et al. 1999; Chen et al. 2004) but not listed in Yang et al. (2002) are also included in this work for comparison. Table 1 is the basic properties of the detected YSCs. Column 1 represents the names of IRAS sources. Columns 3 and 4 are the central position of the YSCs. Column 5 presents the adopted distance of each region. To compare our data homogeneously, we generally use the kinematic distance derived from Yang et al. (2002). A few regions have unreasonably large or have more than one or no solution of kinematic distance. In such

cases we use galactic model of Jones et al. (1981) and the star-counting method to estimate the distances. In those regions that both have unambiguous kinematic and star-counting distance, we find that they agree within 50%. Column 6 is the identifications that appear in Table 1 of Bica, Dutra, & Barbuy (2003). We define that our clusters are associated with that of Bica, Dutra, & Barbuy (2003) if the central positions are different by less than the angular size of the corresponding clusters. Totally 15 clusters are found their identification in Bica, Dutra, & Barbuy (2003).

Figs. 1 presents the results of the survey, among which only the IRAS 02232+6138 region is shown in the printed article as a sample, while others are available in electronic edition of the Journal. The upper-left panels show the color images of the regions. Most of the color images are composed of JHKs-band images, but in some regions (IRAS06142, 06306, 06437, 06548) where there are not H-band data, the color images are composed of JKs- and I- band images, which are downloaded from the Digital Sky Survey in the Centre de Données astronomiques de Strasbourg<sup>1</sup>. All regions presented show congregations of stars in different morphologies, suggesting that they are probably young stellar clusters or groups. Since these regions have different distances from the Sun, so that the detection limit are different, we do not intend to make any definition between clusters or groups. All these regions will be called YSCs. The stellar contents of the YSCs have different colors. According to their colors, we classify them into three categories: 1) embedded: nearly all stars cannot be seen in the optical; 2) partially embedded: some part of the cluster can be detected in the optical; 3) optical: nearly all members can be detected in the optical. This kind of classification probably reflects the evolutionary sequence of the YSCs.

The upper-right panels display the surface density maps of stars that are detected in the Ks-band. The maps further show that in every region, there is a density peak that surpasses

---

<sup>1</sup>The data can be accessed at the web site <http://cdsweb.u-strasbg.fr/>

the surrounding areas by more than 3 times of the standard deviation. In most regions the density peaks are positionally coincident with IRAS sources. The morphologies of the peak areas vary from region to region. Generally they can be classified into four categories: spherical, elongated, amorphous and multi-peaked.

The lower-left panels of Fig. 1 show the radial dependence of the surface density in each region. The densities are calculated in concentric annuli with a bin size of  $14.3''$  (15 pixels). The centers are at the positions listed in Table 1. In most regions the surface densities peak at the center and decrease quickly outward. The figures also show the  $r^{-1}$  fit in each region (dash lines). In many regions the surface densities fit the  $r^{-1}$  curve fairly well. This confirms that in these regions there are congregations of stars toward the centers. The distance of the region I05380 is quite small and the regions is relative large in angular size comparing to our field of view. We have not found a reasonable center for this region. Therefore the surface density does not peak at the center we give. From the radial dependence of the surface densities we can roughly determine the radii of the clusters. We define the distance at which the density exceeds twice the terminal densities as the radius of a cluster. The radii of the clusters are listed in Table 2.

It is difficult to identify the cluster members out of the field stars. Fortunately, stars in most regions are concentrated toward the centers, so that the central parts are much denser than outer fields. We use the contour line with its value trice the average density of the outer field as a defining circle within which the detected sources are defined as cluster members. The number of the detected cluster members is calculated based on the above definition, and is listed in Table 2. Since the surface densities of the clusters are much higher than that of the field stars, we presume that the field star contamination does not make statistical significance. We then construct the Ks-band luminosity functions (KLFs) of the regions from above assumption, and show them in the lower-right panels of Fig. 1.

In Table 2 we present the derived properties of the YSCs. Column 2 shows the radii of the clusters defined above. Column 3 is the number of all stars detected at Ks. Column 4 is the Ks-band absolute magnitude of the brightest star. Column 5 indicates the number of stars that are brighter than 0.0 mag in the Ks-band. This column may be suggestive of the number of intermediate to high mass stars. In column 6 and 7 we present the surface densities at the centers of the clusters. In column 6 the densities are calculated for all stars detected at Ks while in column 7 they are calculated for those detected at an uniform completeness limiting magnitude (1.5 absolute mag at Ks). Column 8 and 9 presents the morphologies and color properties of the clusters.

Most of the cluster listed here are embedded or partially embedded in their natal cloud, indicating that they are still very young. It is not surprising since our selection is from those showing CO molecular line emissions. The morphology of the clusters changes from region to region. We roughly classify the morphologies into four categories: round, elongated, multi-peak, and complex. About 51% of the clusters are roughly round in morphology; 15 % show elongated peaks and another 25% have more than one peaks; for the rest regions we cannot describe their morphologies because they have too many peaks in the surface density maps. The estimated radii range from 0.1 parsec to 2 parsecs. The surface densities change over a range of 2 orders for all stars detected. However, when taking the distance into account, i.e., when we use an overall completeness limit (1.5 mag) to calculate the surface densities, the range becomes smaller, from  $\sim 30$  to  $\sim 900$  per square parsec. In order to make a census of massive stars in these regions, we list in column 4 the Ks-band absolute magnitude of the brightest star in each region. Thirty-seven regions contain star(s) brighter than 0.0 mag (the K magnitude of an A0 main-sequence star) and twenty-four regions brighter than -1.9 mag (B0, Tokunaga 1999; Drilling & Ulandolt 1999). Considering most of the YSCs are embedded or partially embedded, so that they are obscured to some extent, the percentage would be still higher. This result suggests that more than one-half of the clusters may contain

massive stars.

## 4. Discussion

### 4.1. Selection Effect

As stated in the introduction section, our sample is only a small part of the Galactic YSCs. It should be kept in mind that any statements based on this work make sense only on limited class of YSCs. Most of our samples are selected from molecular outflow candidates observed by Yang et al. (2002). The outflows that are detected before (Fukui 1989; Wu et al. 1996) are excluded except for the region AFGL 5142 and AFGL 5157. Those outflows cataloged by Fukui (1989) and Wu et al. (1996) may represent the most easily detectable ones in the Galaxy. Our samples, on the other hand, could be less easily detectable outflow regions. Follow-up molecular line observations show that most of the outflow candidates (Yang et al. 2002) are in fact outflows ( $> 80\%$ , Mao & Yang, private communications). There might be two main reasons that makes the outflows less easily observable. One is that the outflows have larger distances from the sun, so that the outflows are apparently weaker. The other reason is that the outflows are intrinsically weak. The latter may represent more evolved status of the cluster. Comparison of our clusters to those by Hodapp (1994) show that the average distance of the former is two times larger than that of the latter, suggesting that the former reason could be more plausible.

These clusters are roughly randomly distributed over  $70^\circ$ – $240^\circ$  galactic longitude. All the galactocentric radii are great than 8.0 kpc, the assumed distance between the galactic center and the sun, except for the region IRAS20190+4102. Therefore the statistics based on this work may represent to some extent the properties of those YSCs beyond the solar circle.

## 4.2. Numbers of Members

Fig. 2 shows the distribution of the number of cluster members. It is interesting that a majority of clusters are relatively “poor”, i.e., most of them have members less than 100. Only 4 clusters (8.5%) have more stars than 200. We note however, the numbers are calculated from the stars that are detected in the Ks-band. Many of the samples have large distances that prevent us from detecting the low-mass stars and brown dwarfs. Whether it is a typical property of the YSCs in the outer Galaxy may need further investigation.

Even at present detection limit, we find that stellar members of the YSCs ( $\sim 70$ ) are much more than that of typical galactic open clusters ( $\sim 14$ , Lyngå, 1987). These numbers are at least two orders lower than those of globular clusters. Therefore, a majority of our YSCs is likely going to evolve into open clusters by ejecting their members into the space and finally dissolved in the galactic stellar field.

## 4.3. Linear Sizes

In Fig. 3 we present the radius frequency of our samples. A majority of the YSCs have radii  $\sim 0.2$ – $0.8$  pc, with a peak at 0.4 pc. Still a few of them are larger with radii exceeding 1.0 pc. Since our samples are relatively “poor”, the vast majority of the YSCs will evolve into open clusters and disperse eventually. The linear size of an unbounded YSC is expected to get larger and larger as it evolves dynamically. Therefore more or less the radius of a YSC reflects its evolutionary status.

#### 4.4. Stellar Surface Densities

Fig. 4 presents the distribution of stellar surface densities calculated from all stars detected (grey histograms) and those stars brighter than 1.5 absolute magnitude. The figure shows that a number of YSCs are quite densely populated with surface densities greater than  $1000 \text{ pc}^{-2}$ , making up a percentage of 25%. These clusters are mainly located within 1 kpc from the sun. Some other YSCs would be of similar surface densities if we take detection limit into consideration, so that the percentage would be higher.

To compare the stellar surface densities among the YSCs, we calculate them excluding those stars fainter than 1.5 absolute magnitude, the overall completeness limit for all regions. The data set is also presented in Fig. 4 (hatched histograms). Unlike the data set for all detections, the data set of limited detections is regularly distributed. Using exponential curve we can fit the distribution quite well. There could be two possibilities to account for the feature. Assuming clusters and stars are formed steadily, and the initial surface densities are uniform, the fast drop of the surface densities would suggest a quick dynamical dispersion of clusters in their early ages. The other possible reason is that a majority of the clusters are born in a relatively loose environment. Which one is more likely needs further investigation.

#### 4.5. Ks-band Luminosity Function

A KLF is a fine indicator of the initial mass function (IMF) in young stellar clusters, although the conversion function may be complicated and depend upon star formation history (e.g. Muench et al. 2000; Muench et al. 2002). However, individual clusters usually have small numbers of members that make the KLFs have large statistical fluctuations. Clustering is believed to be a major star forming mode in the Galaxy. The final mass function will depend upon the formation and evolution of all clusters in the Galaxy. We thus construct

the KLF for all clusters of our sample.

Fig. 5 presents the Ks-band luminosity function of all stars in all regions (grey histograms). All the magnitudes are converted to absolute scale using the adopted distances listed in Table 1. Due to the difference of the distance in each region, the completeness limiting magnitudes are also different from region to region. The overall completeness limiting magnitude is estimated from the one in the most distant region, i.e., IRAS 06073+1249. We adopt 1.5 mag as the completeness limiting magnitude of the whole data, although in some regions the completeness limits are far above that value.

Some features can be obtained from the first look at the figure. The numbers at each bin increase constantly towards the fainter end until well beyond the estimated completeness limit at 1.5 mag. The rising part of the histogram is roughly linear. A linear fit between -4.0 and 1.5 mag range shows that the slope is  $\sim 0.36$ . This value is quite close to the ones derived from some single YSCs such as Trapezium (0.39, Hillenbrand 1997; Zinnecker et al. 1993) and NGC1333 (0.4, Lada & Lada 1995) but significantly larger than field stars (0.26, Lada et al. 1991). This result suggest that the YSCs in the outer Galaxy as a whole may be formed in quite similar environments.

Generally speaking, the brighter section of the KLF is not affected by the distances of the clusters. We present in Fig. 5 the KLF selected for clusters with distances between 0.5–2.5 kpc (hatched histograms). Apart from the fact that the peak of the KLF is shifted to the fainter end, its shape does not change much from that for all clusters. Its slope (0.37) is also quite close to that for all clusters.

We have modelled the KLF of the selected clusters with Monte Carlo approach as described in Muench et al. (2000). We assume the IMF as  $dN_m = m^{-\alpha} dm$ , where  $\alpha = -0.4$  when  $0.02M_{\odot} \leq m \leq 0.08M_{\odot}$ , 1.2 when  $0.08M_{\odot} \leq m \leq 1.0M_{\odot}$ , and 2.7 when  $m \geq 1.0M_{\odot}$  (Kroupa 2002, and references therein). A uniform distribution with an average 3 Myr age

and 5 Myr spread is presumed for the star formation history of these clusters. The Monte Carlo simulation to the observed KLF of the selected YSCs is shown as dash curve in Fig. 5. The model KLF fits the observed one quite well, suggesting that the IMF of the YSCs could be in a similar form.

Fig. 5 also indicates that the KLFs ascend along the linear fitting lines towards the fainter end, departing from the lines nearly at the completeness limits. Both the KLFs peak at 1 mag fainter than the completeness limits. Since the completeness limit is estimated for 90% detections, and the typical values is used instead of the lowest value, The turning of the KLF curve for the selected regions is only considered marginal but not concrete conclusion. The actual turning point, if exists, should await future deeper observations.

#### 4.6. High-mass Stars

Column (4) of table 2 shows that number of stars that are brighter than 0.0 absolute magnitude at Ks. These stars are possibly intermediate- to high-mass ones. Thirty-seven (79%) out of the listed regions contain one or more stars brighter than a A0 main-sequence star. Considering that the magnitudes are not extinction-corrected, the percentage could be still larger. This suggests that most of the YSCs may contain at least intermediate-mass stars. Twenty-four (51%) regions are found to contain stars brighter than a B2 main-sequence star. It implies that more than one-half of the YSCs may contain high-mass stars with mass greater than  $10 M_{\odot}$ .

Fig. 6(a) displays the plots of the Ks magnitude of the brightest source in each region against the number of the cluster members. In order to minimize the artificial effects resulting from the different completeness limit, we choose those regions with distances between 0.5–2.5 kpc, and count only the numbers of members with  $M_K$  brighter than 3.5 mag (the

completeness limit for a distance of 2.5 kpc). A weak trend can be noticed that the brightness of the main source rises with the number of members within the completeness limit until  $n \sim 200$ . Since in the pre-main-sequence stage intermediate- to high-mass stars do not change their luminosities dramatically as lower-mass ones do (e.g. Palla & Stahler 1993), the mass rather than evolutionary stage is important to determine the luminosity of a high-mass star. The K magnitudes of the brightest sources thus reflect their masses. This result suggests the mass of the most massive star in a cluster is related to the numeric abundance of the cluster, which confirms the result by Testi et al. (1997).

Fig. 6(b) displays the Ks magnitudes of the main sources against the radii of the clusters. Since the estimation of radius does not strongly depend on the distance, we do not exclude the samples with large distances. The plots are distributed at the upper-left corner of the frame. There seems to be a critical line below which plots are forbidden. The result suggests that given a radius of a cluster, the mass of the most massive star in the cluster is expected to be larger than a critical value.

In Fig. 6(c) we present the plots of Ks magnitude of the main source against the estimated stellar surface density. Again, we exclude those regions with distances greater than 2.5 kpc and those stars fainter than  $M_K \sim 3.5$  mag for the statistics. The plots are distributed randomly in the frame, indicating that the Ks magnitude is not well-related to the surface density. We conclude that the mass of the most massive stars in a cluster is more related to the number and the radius than to the surface density of the cluster.

## 5. Summary

We conducted a near-infrared (JHKs) survey towards the CO molecular outflow candidate regions listed in Yang et al. (2002). About one-third of the listed regions have been

observed, we detected 45 clusters or stellar groups. The main results are summarized as following:

1. We present the color images composed of JHKs images, the surface density maps, radial density profiles and KLFs of the YSCs. Most of the clusters are still embedded in their natal cloud, so that a fraction or all of the stars in them cannot be detected in the optical. These clusters show different near infrared colors, indicating that they could be in different evolutionary stage. The morphologies of the clusters are also different. According to the shape of the surface density maps, we can roughly classify them as spherical, elongated, amorphous and multi-peaked. We also show the radial dependence of the surface density of each region, from which we can estimate the rough linear size of each cluster. Most of the surface density profiles are fitted quite well to a  $r^{-1}$  curve.
2. The number of stars in each cluster varies from ten to several hundred. A majority of the clusters are relatively “poor”, i.e., the numbers of members of the clusters are mostly below 100. However, this result should be noted in caution because the completeness limits are different from region to region due to the different distances. The surface densities of the clusters vary by more than an order, even they are estimated at the same completeness limit.
3. We have constructed the K-band luminosity function of the stars in all clusters as well as in the clusters with distances between 0.5–2.5 kpc. The slope of the linear part of the KLFs are quite similar to those of the YSCs such as the Trapezium and NGC 1333, but is significantly larger than that of the field stars. Monte Carlo simulation of the KLF of the selected clusters suggests the IMF of the clusters could be in a similar form.
4. About three-fourths of clusters may contain intermediate- to high-mass stars, and

one-half of the clusters may contain high-mass stars. A plot of the Ks-band absolute magnitudes of the brightest sources in each cluster against the numbers of the cluster members suggests a possible correlation between the mass of the most massive star and the number of the cluster members. A plot of  $M_K$  against the radius suggests given the radius of a cluster, the mass of the main source can be expected to be larger than some critical value. The mass of main source seems to be less correlated with the surface density of each cluster.

The authors are willing to express thanks to the staffs of the Okayama Astrophysical Observatory for their kind help during the observations. We would also like to acknowledge Drs Y. Yao, H. Wang and M. Ishii for using their telescope time to obtain part of the data, and for their instructions to reduce the data. This work is supported by NSFC No. 10473022 and 10133020, and Ministry of Science and Technology G19990754. This research has made use of the SIMBAD database, operated at CDS, Strasbourg, France, the USNOFS Image and Catalogue Archive operated by the United States Naval Observatory, Flagstaff Station, as well as the 2MASS data base.

## REFERENCES

- Bica, E., Dutra C.M., & Barbuy B., 2003, *A&A*, 397, 177
- Chen, Y., Yao, Y., Yang, J., Hirao, T., Ishii, M., Nagata, T., & Sato, S. 1999, *AJ*, 117, 446
- Chen, Y. et al. 2004, in preparation
- Tokunaga 1999, in *Allen's Astrophysics Quantities*, 4th ed. ed. A.N. Cox, (Springer), 151
- Drilling, J.S., & Landolt, A.U. 1999, in *Allen's Astrophysics Quantities*, 4th ed. A.N. Cox, (Springer), 389

- Fukui, Y. 1989, in Proceedings of the ESO Workshop on Low Mass Star Formation and Pre-main
- Greene, T.P., & Meyer, M.R. 1995, *ApJ*, 450, 233
- Hillenbrand, L.A. 1997, *AJ*, 133, 1733
- Hodapp, K.W., 1994, *ApJS*, 94, 615
- Hunt, L. K., Mannucci, F., Testi, L., Migliorini, S., Stanga, R. M., Baffa, C., Lisi, F., & Vanzi, L. 1998, *AJ*, 115, 2594
- Jiang, Z. et al. 2002, *ApJ*, 577, 245
- Jiang, Z. et al. 2003, *ApJ*, 596, 1064
- Jones, T.J., Ashley, M., Hyland, A.R., & Ruelas-Mayorga, A. 1981, *MNRAS*, 197, 413
- Kroupa, P., 2002, *Science*, 295, 82
- Lada, C.J. 1999, in *The Origin of Stars and Planetary Systems*, eds C.J. Lada and N.D. Kylafis, (Kluwer Academic Publishers 1999), p. 143
- Lada, C.J., DePoy, D.L., Merrill, K.M., & Gatley, I. 1991, *ApJ*, 374, 533
- Lada, C.J., & Lada, E.A. 2003, *ARA&A*, 41, 57
- Lada, E.A. & Lada, C.J. 1995, *AJ*, 109, 1682
- Lyngå, G. 1987, *Catalogue of Open Cluster Data*, 5th ed. (computer-based catalog distributed by NASA Data center)
- Mermilliod, J. C. 1995, in *Information and On-Line Data in Astronomy*, ed. D. Egret, & M. A. Albrecht (Dordrecht: Kluwer), 127

- Muench, A.A., Lada, E.A., & Lada, C.J. 2000, ApJ, 533, 358
- Muench, A.A., Lada, E.A., Lada, C.J., & Alves, J. 2002, ApJ, 573, 366
- Okumura, S., Nishihara, E. & Watanabe, E. 2000, PASJ, 52, 931
- Palla, F., & Stahler, S.W. 1993, ApJ, 418, 414
- Porras, A., Christopher, M., Allen, L., Di Francesco, J., Megeath, S.T., & Myers, P.C., 2003, AJ, 126, 1916
- Salpeter, E.E. 1955, ApJ, 121, 161
- Scalo, J. 1998, in ASP Conf. Proc. 142, 38th Herstmonceux Conference: The Stellar Initial Mass Function, ed. G. Gilmore and D. Howell (SanFrancisco: ASP), 201
- Testi, L., Palla, F., Prusti, T., Natta, A., & Maltagliati, S. 1997, A&A, 320, 159
- Wu, Y., Huang, M., & He, J. 1996, A&A Supp. Ser., 115, 283
- Yang, J., Jiang, Z., Wang, M., Ju, B., & Wang, H. 2002, ApJS, 141, 157
- Zinnecker, H., McCaughrean, M.J., & Wilking, B.A. 1993, in: Levy, E.H., Lunine, J.I. (eds) Protostars and Planets III, p. 429, Arizona

Table 1:: Basic data of the detected YSCs

IRAS	Association	$\alpha_{2000}$	$\delta_{2000}$	D(kpc)	Identification
02232+6138	RAFGL 331	02:27:08	+61:52:32	5.6	BDB17
02245+6115	...	02:28:22	+61:28:34	5.8	BDB20
02455+6034	...	02:49:04	+60:43:19	4.8	...

Table 1:: Continued

IRAS	Association	$\alpha_{2000}$	$\delta_{2000}$	D(kpc)	Identification
02593+6016	RAFGL 416	03:03:15	+60:27:48	3.8	BDB34
03101+5821	...	03:14:05	+58:33:08	4.2	...
03235+5808	RAFGL 5095	03:27:31	+58:19:21	6.0	...
04000+5052	X0359+508	04:03:50	+51:00:52	5.0	...
04324+5106	RAFGL 5124	04:36:21	+51:12:53	6.5	BDB59
04547+4753	RAFGL 5133	04:58:30	+47:58:25	2.3	...
04575+4647	...	05:01:17	+46:51:52	4.2	...
05044-0325	CED 040	05:06:58	-03:21:14	0.7	...
05274+3345	RAFGL 5142	05:30:47	+33:47:52	1.8	...
05345+3157	RAFGL 5157	05:34:48	+31:59:27	1.8	BDB65
05352+2725	...	05:38:23	+27:26:54	4.1	...
05359+3003	...	05:39:12	+30:03:54	0.7	...
05361+3539	...	05:39:28	+35:40:46	1.8	BDB83
05375+3540	...	05:40:53	+35:41:43	1.7	BDB86
05380+3608	...	05:41:18	+36:09:57	2.0	...
05391-0152	...	05:41:38	-01:53:59	0.7	...
05439+3035	X0544+305A	05:47:13	+30:36:12	1.8	BDB97
05554+2013	X0555+202	05:58:25	+20:13:55	1.8	...
06046-0603	LDN 1646	06:07:08	-06:03:36	0.8	BDB101
06073+1249	RAFGL 5185	06:10:12	+12:48:47	6.7	BDB115
06099+1800	RAFGL 896	06:12:55	+17:59:24	0.9	BDB120
06102+1537	...	06:13:02	+15:36:12	3.3	...
06105+1756	S258	06:13:28	+17:55:30	0.9	BDB123

Table 1:: Continued

IRAS	Association	$\alpha_{2000}$	$\delta_{2000}$	D(kpc)	Identification
06114+1745	RAFGL 5188	06:14:23	+17:44:41	0.9	BDB124
06117+1350	S269	06:14:37	+13:49:36	3.8	...
06134+2348	...	06:16:35	+23:46:18	0.6	...
06142+1439	X0614+146	06:17:05	+14:37:47	2.2	...
06227+2001	S253	06:25:44	+19:59:48	4.0	...
06306+0437	...	06:33:16	+04:35:04	1.1	BDB131
06437+0009	...	06:46:16	+00:06:25	6.2	...
06548-0815	BFS 63	06:57:17	-08:19:55	0.8	...
07017-1114	RAFGL 5220	07:04:08	-11:18:59	0.5	BDB149
07033-1033	...	07:05:43	-10:38:06	1.0	...
07299-1651	RAFGL 5234	07:32:10	-16:58:16	1.0	...
20190+4102	...	20:20:47	+41:12:08	2.8	...
20205+3948	...	20:22:22	+39:58:07	3.8	...
21008+4700	LDN 0954	21:02:32	+47:12:35	5.5	...
22475+5939	S146	22:49:29	+59:54:51	4.2	...
22566+5830	S152	22:58:40	+58:46:54	4.6	...
23026+5948	BFS 15	23:04:45	+60:04:34	4.7	...
23134+6131	S161B	23:15:41	+61:47:45	4.4	...
23138+5945	RAFGL 3057	23:16:03	+60:01:59	3.4	...
23385+6053	...	23:40:57	+61:10:41	4.2	...
23545+6508	RAFGL 5623	23:57:06	+60:27:48	1.3	...

Table 2:: Derived properties

Region	R	Num <sup>a</sup>	K <sub>min</sub> <sup>b</sup>	N <sub>A0</sub> <sup>c</sup>	Surface Density		Morph.	Prop.
	(pc)		(mag)		All <sup>d</sup>	Lim <sup>e</sup>		
(1)	(2)	(3)	(4)	(5)	(6)	(7)	(8)	(9)
02232+6138	1.55	171	-4.62	36	58.9	58.9	L	E
02245+6115	0.68	66	-3.47	8	41.2	41.2	L	E
02455+6034	0.44	138	-3.66	26	35.1	35.1	M	PE
02593+6016	1.41	138	-2.61	5	103.9	48.0	R	E
03101+5821	0.59	78	-2.31	9	39.3	26.2	R	E
03235+5808	1.40	145	-3.19	14	25.6	25.6	R	E
04000+5052	0.93	51	-3.85	3	64.6	60.0	R	PE
04324+5106	1.81	129	-2.81	16	38.2	38.2	M	E
04547+4753	0.63	77	-0.50	1	414.5	152.7	R	PE
04575+4647	1.16	66	-2.43	4	39.3	32.7	L	PE
05044-0325	0.16	26	-0.92	4	1413.2	471.1	R	PE
05345+3157	0.50	96	-0.90	2	534.3	35.6	R	E
05352+2725	0.67	82	-0.81	4	569.9	142.5	R	PE
05352+2725	0.57	51	-2.62	11	41.2	27.5	L	E
05359+3003	0.07	35	2.96	0	1648.7	235.5	R	E
05361+3539	0.25	44	-0.99	2	285.0	71.2	R	PE
05375+3540	1.03	292	-2.40	6	958.4	159.7	M	PE
05380+3608	0.19	68	-0.61	2	115.4	57.7		PE
05391-0152	0.27	123	-3.37	8	2119.8	942.1	R	E
05439+3035	0.21	71	-1.89	2	249.3	106.9	L	E
05554+2013	0.21	32	-0.18	1	249.3	142.5	R	E

Table 2:: Continued

06046-0603	0.22	48	1.44	0	1082.0	180.3	M	PE
06073+1249	1.71	77	-3.12	16	30.9	30.9	R	PE
06099+1800	0.24	131	1.17	0	3277.1	285.0	R	PE
06102+1537	0.93	67	-0.82	1	95.4	31.8	L	PE
06105+1756	0.22	76	1.07	0	1852.3	142.5	R	PE
06114+1745	0.13	41	0.39	13	135.9	95.9	M	PE
06117+1350	1.24	329	-2.20	0	2244.1	320.6	M	PE
06134+2348	0.06	18	1.68	0	1567.3	285.0	M	PE
06142+1439	0.15	13	1.67	0	143.1	23.8	R	PE
06227+2001	0.55	23	-0.27	2	28.9	21.6	M	PE
06306+0437	0.20	49	-0.62	3	667.7	95.4		E
06437+0009	1.01	32	-5.37	11	24.0	24.0	R	PE
06548-0815	0.11	18	1.58	0	1803.3	180.3	E	PE
07017-1114	0.06	43	0.44	0	3231.5	461.6	R	PE
07033-1033	0.09	42	0.01	0	577.1	230.8	M	PE
07299-1651	0.22	69	-2.28	1	1846.6	230.8	R	E
20190+4102	0.13	13	-1.90	2	117.8	44.2	L	O
20205+3948	0.35	33	-2.16	8	111.9	111.9	R	PE
21008+4700	0.26	45	-4.12	13	34.3	30.5		PE
22475+5939	0.69	144	-3.35	12	137.4	98.1	R	PE
22566+5830	0.85	85	-2.75	31	92.7	70.9	R	PE
23026+5948	0.66	137	-4.19	19	78.4	78.4	M	PE
23134+6131	0.31	58	-3.43	11	53.7	41.7	R	PE
23138+5945	1.11	213	-4.12	19	179.7	109.8	R	PE

Table 2:: Continued

23385+6053	0.39	22	-0.14	2	45.8	32.7	M	PE
23545+6508	0.29	84	-2.00	2	819.5	68.3	M	PE

abbreviations: L–elongated; R–round; M–multi-peaks; E–embedded; PE–partially embedded; O–optical

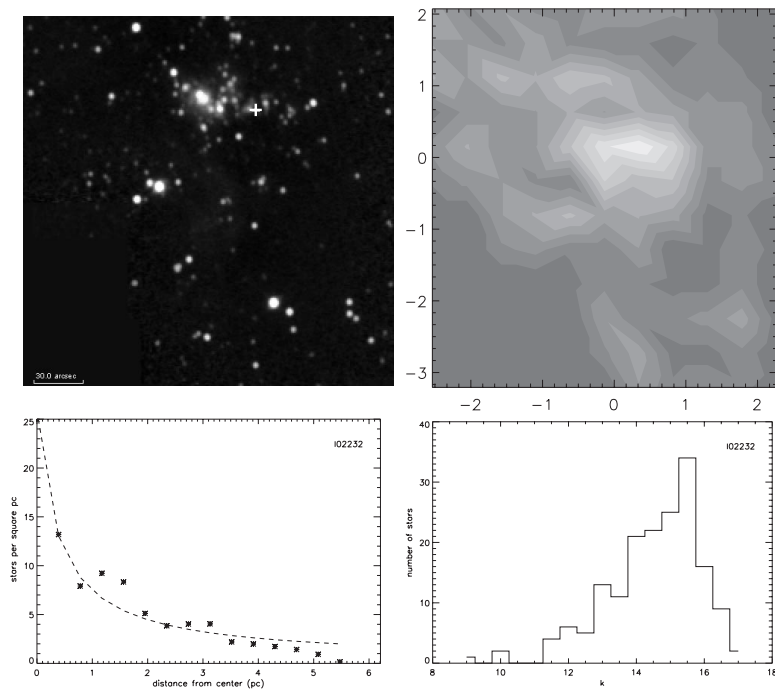
<sup>a</sup> Number of stellar member detected at Ks;

<sup>b</sup> Absolute Ks magnitude of the brightest source;

<sup>c</sup> Number of stars brighter than absolute 0.0 mag at Ks;

<sup>d</sup> Calculated for all detected stars at Ks;

<sup>e</sup> Calculated for stars detected at a uniform completeness limiting magnitude



IRAS02232+6138

Fig. 1.— Upper-left panels: The color images of the regions. Most of the color images are composed of JHKs images, but a few of them are composed of IJKs images (see text). The plus signs represent the position of IRAS sources. Upper-right panels: Surface density maps of the region. All stars that are detected in the Ks-band are used to construct the maps. A bin-size of 30 pixels with 20 pixel separation is used to calculate the surface density. Lower-left panels: Radial dependence of the surface densities. The surface densities are calculated in a series of concentric circles with a bin-size of 20 pixels. Lower-right panels: The K-band luminosity function of the region. The bin-size is set to 0.5 mag. The names of the regions are shown at the bottoms of the frames. The figure for IRAS 02232+6138 is a sample of the whole set of the graphics. Others are presented in electronic edition of the Journal.

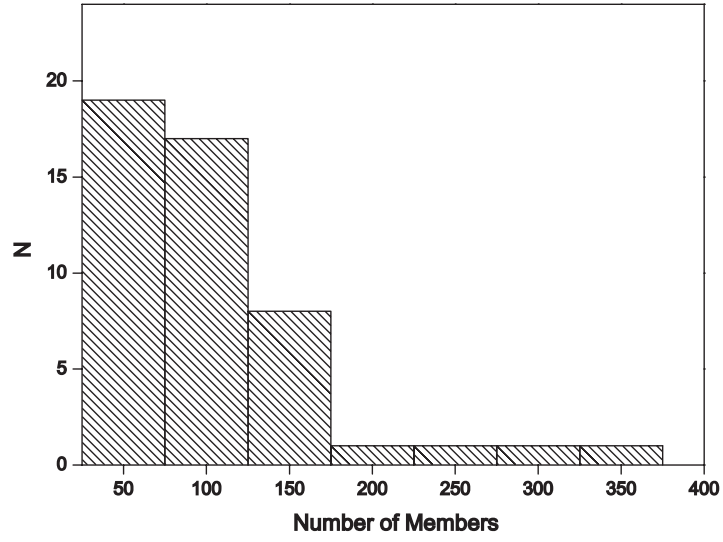


Fig. 2.— Distribution of the numbers of the cluster members. The numbers are estimated from all that are detected in the Ks-band.

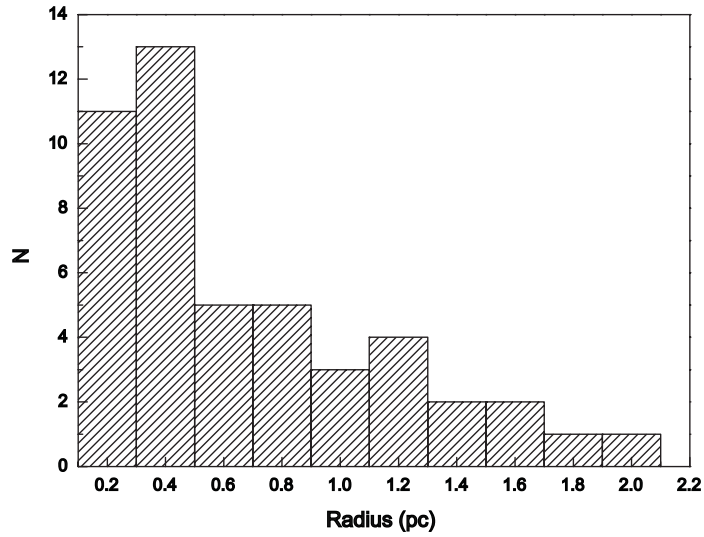


Fig. 3.— Radius frequency of the samples.

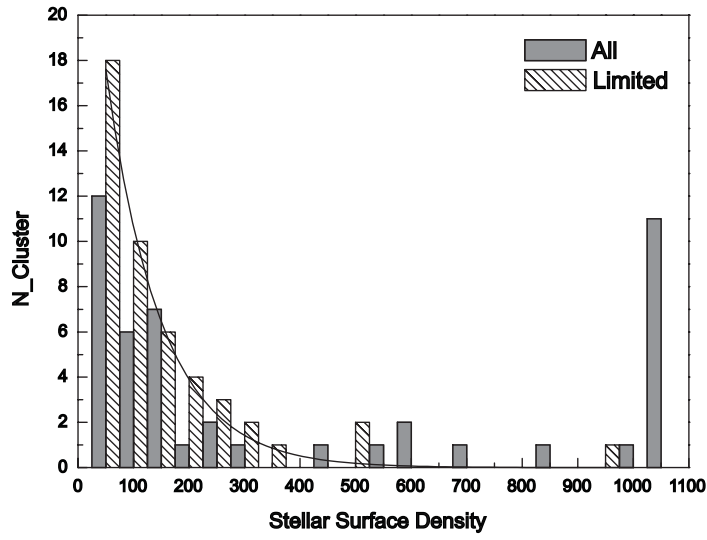


Fig. 4.— Distribution of Stellar surface density. Grey histograms are calculated with s-stars detected in the Ks-band. Hatched histograms are for stars brighter than 1.5 absolute magnitude. Solid curve is the exponential decay fit to the latter data set.

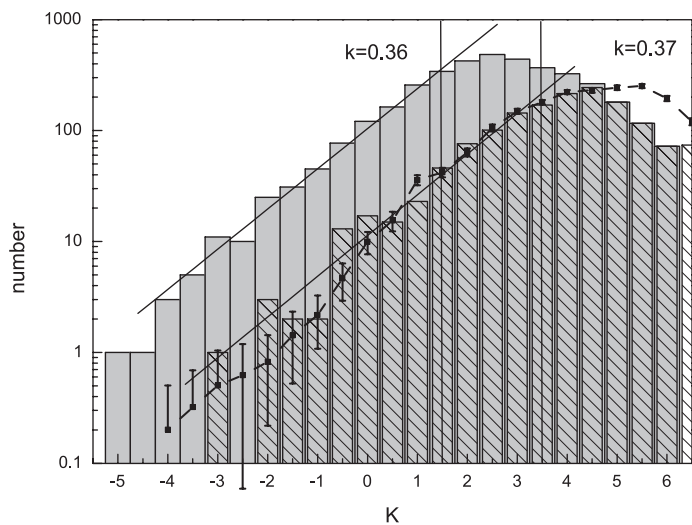


Fig. 5.— Ks-band luminosity functions of all clusters (grey histograms) and clusters with distances less than 2.5 kpc (hatched histograms). The abscissa is the absolute magnitude with a bin size of 0.5 mag. The vertical solid lines are the completeness limiting magnitudes at 6.7 kpc (1.5 mag) and 2.5 kpc (3.5 mag), respectively. The slanting lines are linear fits of the corresponding KLFs. The dash curve represents the Monte Carlo simulation to the observed KLF of the selected clusters.

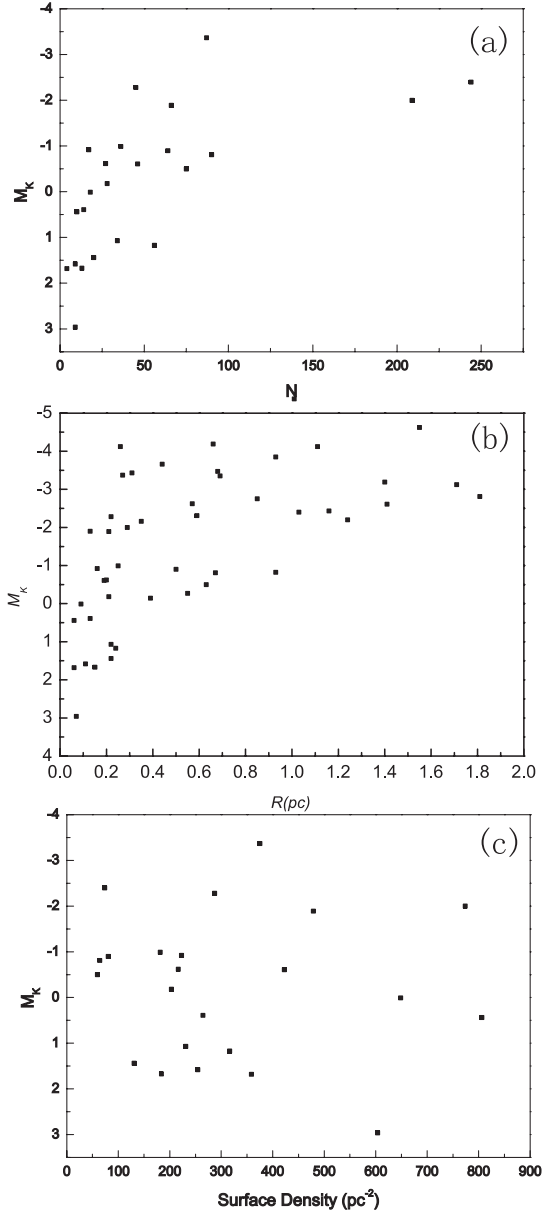


Fig. 6.— (a) Plot of the K magnitude ( $M_K$ ) of the brightest source against the number ( $N$ ) of the cluster members. (b) Plot of  $M_K$  against the radius of the clusters. (c) Plot of  $M_K$  against the stellar surface density in the cluster. To minimize the artificial effects resulting from the different completeness limit, we exclude regions with distance greater than 2.5 kpc and sources fainter than  $M_K \sim 3.5$  mag when constructing panel (a) and panel (c).